

Joint Chromatic and Polarimetric Demosaicing via Sparse Coding

Sijia Wen^{1,3} Yinqiang Zheng² Feng Lu^{1,3*} Qinqing Zhao^{1,3}

¹Beihang University ²National Institute of Informatics ³Peng Cheng Laboratory
 {sijiawen, lufeng}@buaa.edu.cn yqzheng@nii.ac.jp zhaoqp@vrlab.buaa.edu.cn

Abstract

Thanks to the latest progress in image sensor manufacturing technology, the emergence of the single-chip polarized color sensor is likely to bring advantages to computer vision tasks. Despite the importance of the sensor, joint chromatic and polarimetric demosaicing is the key to obtaining the high-quality RGB-Polarization image for the sensor. Since the polarized color sensor is equipped with a new type of chip, the demosaicing problem cannot be currently well-addressed by former methods. In this paper, we propose a joint chromatic and polarimetric demosaicing model to address this challenging problem. To solve this non-convex problem, we further present a sparse representation-based optimization strategy that utilizes chromatic information and polarimetric information to jointly optimize the model. In addition, we build an optical data acquisition system to collect an RGB-Polarization dataset. Results of both qualitative and quantitative experiments have shown that our method is capable of faithfully recovering full 12-channel chromatic and polarimetric information for each pixel from a single mosaic input image. Moreover, we show that the proposed method can perform well not only on the synthetic data but the real captured data.

1. Introduction

Conventional color imaging can sample spectral information. Polarization imaging considers the electric field as a vector which is contained in a plane perpendicular to the direction of propagation. It is a way to analyze the particular direction of the oscillation of the electric field described by the light. Color is easily perceptible to human eyes and is at the core of numerous computer vision problems. On the contrary, polarization is invisible to our eyes, yet it usually conveys critical information on intrinsic material properties,

*Corresponding author.

such as reflectance and external surface geometry.

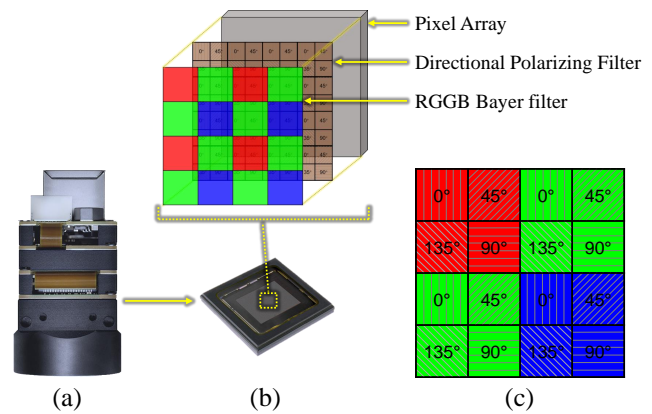


Figure 1. The polarized color sensor: (a) The latest polarimetric RGB camera by Lucid Vision, which is equipped with a Sony IMX250MYR CMOS sensor; (b) The polarized color sensor with an RRGB Bayer filter [5] in addition to the directional polarizing filter to form a 4×4 array; (c) The RGB-Polarization pattern of IMX250MYR which can simultaneously capture RGB chromatic and polarimetric information in the mosaic form.

Previously, we could only get either chromatic information or polarimetric information of the scene by each snapshot. Various existing approaches [39, 21, 25, 47] have been proposed for chromatic demosaicing. Similarly, the Division-of-Focal-Plane (DoFP) polarimeters have evolved a lot for snapshot polarimetric imaging. Therefore, polarimetric demosaicing methods [50, 51, 20, 49, 44, 19] have been proposed to reconstruct full resolution polarization images.

Until recently, thanks to the latest progress in image sensor manufacturing technology, the new released single-chip polarized color sensor (PHX050S camera by Lucid Vision Labs) is able to simultaneously capture RGB and polarization pixels of the scene in the mosaic form. This camera is equipped with an RRGB Bayer filter in addition to the directional polarizing filter to form a 16 pixels calculation unit as the RGB-Polarization pattern, as shown in Fig. 1.

Joint chromatic and polarimetric demosaicing for this single-chip polarized color sensor can be a benefit to a great variety of computer vision tasks. For example, inspecting colorful objects such as various fruits and vegetables, LCD panels or mobile phone displays can benefit from reflection removal while maintaining the shape and color integrity of the object in the image. Joint chromatic and polarimetric demosaicing can also ease the procedure of sugar concentrations measuring in industry, as shown in Sec. 5.4. It explains that joint chromatic and polarimetric demosaicing is indispensable, otherwise, none of the above-mentioned benefits can be achieved. However, as a new type of array pattern, there are no any dedicated demosaicing methods for the polarized color camera.

In this paper, we introduce this novel task into the computer vision community. Restoration of high-quality 12-channel images from the mosaic observations is a highly ill-posed problem. To resolve this issue, we collect the RGB-Polarization dataset by building an optical data acquisition system. The system uses a three-CMOS prism-based RGB camera, which is equipped with a mechanically motorized linear polarizer. Based on the pattern of the single-chip polarized color sensor, we propose a joint chromatic and polarimetric demosaicing model. Considering the lack of data and getting rid of training time, we propose a sparse representation-based optimization strategy by jointly considering chromatic and polarimetric information. Experimental results have shown that our proposed methods are capable of faithfully recovering full RGB chromatic and polarimetric images from a single mosaic input. In summary, we present the following contributions:

- We are the first to introduce the task of joint chromatic and polarimetric demosaicing into the computer vision community and propose a joint chromatic and polarimetric demosaicing model for the RGB-Polarization pattern;
- We propose a custom optimization strategy for the cross interpolation of chromatic and polarimetric information based on the single-chip polarized color sensor;
- We build a data acquisition system to collect a full 12-channel RGB-Polarization dataset, which will be publicly available to facilitate further research.
- The proposed approach is able to achieve state-of-the-art results on both the effectiveness and quality while consuming a short time.

2. Related work

Since image demosaicing is an important and well-studied problem, plenty of researches have been reported

and most of them focus on either image quality improvement or applying it to specific applications [34, 30]. Image demosaicing can be further divided into the RGB-based methods, the polarization-based methods, and joint chromatic and polarimetric methods. In this section, we overview all these categories as related works.

RGB chromatic demosaicing. RGB chromatic demosaicing aims to reconstruct a full 3-channel RGB image from the spatially under-sampled color information recorded by the CFA [40]. Traditional color demosaicing algorithms rely on frequency domain analysis [4, 15, 35], interpolation with hard-coded heuristics [33, 52, 28], spatial self-similarities [7, 53], optimization schemes [9, 32], and compressive sensing [39, 42, 11].

More recently, demosaicing strategies based on neural networks lead to better quality and efficiency. Kappa *et al.* [29] and Go *et al.* [23] are among the first to use neural networks for color demosaicing. Long *et al.* [38] later proposed an adaptive scheme to improve performance. Heinze *et al.* [25] proposed a multi-frame demosaicing algorithm using a neural network to infer the pixel color based on its surroundings. Wang [47] used 4×4 patches to train a multilayer neural network while minimizing a suitable objective function. Gharbi *et al.* [22, 26] constructed a dataset with hard cases, which were used to train a CNN for joint demosaicing and denoising. Heide *et al.* [24] later organized the principles of algorithm design in FlexISP into ProxImaL, a domain specific language for optimization based image reconstruction. Chen *et al.* [8] provides high-quality RGB images from single raw images taken under low-light conditions, but this method cannot be applied to RGB color images.

Polarimetric demosaicing. Demosaicking is performed on each sparse channel to obtain an estimated image with four fully-defined channels, among which three are estimated at each pixel. Snapshot polarization imaging has gained popularity due to the recent advancements in producing micro DoFP polarimeters, with successful applications in analyzing the light electric field oscillation direction [41], material classification [27], 3-D surface reconstruction [14], dehazing [18], and biomedical imaging [3].

A few methods have been proposed to address the demosaicing issue in the polarimetric domain. Bilinear interpolation was first investigated by Ratliff *et al.* [44] who also proposed an extension of the bilinear interpolation. Tyo *et al.* [46] developed a new method to reconstruct the first three Stokes parameters directly from the mosaicked image. Zhang *et al.* [49] took advantage of the correlations in PFA to enhance the spatial resolution. Moreover, a new interpolation method for DoFP imaging sensors with intensity correlation was presented in [2]. A demosaicing model based on sparse representation is proposed in [50]. A customized polarization demosaicing convolutional neural net-

work (PDCNN) was recently presented in [51].

In spite of the fact that numerous researches have been conducted for demosaicing in the color or polarization domain, there does not exist any methods for joint chromatic and polarimetric demosaicing, which is the major target in this paper.

3. Methodology

3.1. Problem Statement

The training phase of deep learning consumes a lot of time. Inspired by the previous demosaicing methods based on sparse representation [50, 39], we propose a joint demosaicing method on the basis of sparse representation. Different from the demosaicing method for microgrid polarimeter imagery or chromatic imagery, the joint chromatic and polarimetric demosaicing need to recover the missing pixels from one out of twelve necessary intensity measurements.

For each channel \mathbf{M}_θ , the observed image is essentially down-sampled from its full-resolution image \mathbf{Y} . Due to the sparse of each channel of the RGB-Polarization mosaic image, the traditional interpolation algorithm cannot recover the image truthfully. Fortunately, we can take advantage of the sparse representation-based method to address this issue. According to sparse representation theory, the joint demosaicing for the polarized color sensor can be transformed to minimize the following problem:

$$\min_{\mathbf{D}_\theta, \mathbf{X}_\theta} \left\{ \sum_{\theta} \|\mathbf{M}_\theta - \text{Mask}_\theta \mathbf{Y}_\theta\|_2^2 + \sum_{\theta} \lambda_{\theta} \|\mathbf{Y}_\theta - \mathbf{D}_\theta \mathbf{X}_\theta\|_2^2 + \rho \|\mathbf{X}_\theta\|_1 \right\}, \quad (1)$$

where Mask_θ represent down-sample matrix based on the RGB-Polarization pattern. $\mathbf{D}_\theta, \mathbf{X}_\theta$ are the dictionary and the corresponding sparse coding. λ, ρ are the parameters to balance the effect of different components.

Sparse representation is essentially composed of dictionary learning and sparse coding. It seems like the problem can directly be solved by learning the dictionary of each channel (\mathbf{D}_θ) and calculating the corresponding sparse coding (\mathbf{X}_θ). However, for some surface materials with complex light transport properties, the full-resolution image might show different colors at different polarizing status. The most obvious example is birefringence, for which an optically anisotropic material has a refractive index that depends on the polarization and the propagation direction of light. In other words, there is a non-negligible correlation between each channel, so λ_θ cannot be set. In addition, simply taking the entire input data as the dictionary is computationally inaccurate and consumes too much storage space. The experimental results in Tab. 3 verify our theory.

Therefore, the correlation between different RGB and polarization channels is key to addressing this interpolation

issue. In this paper, we build a joint demosaicing model to address this challenging problem. In order to optimize this highly non-convex and complicated model, we establish our basic iteration scheme with the idea of ADMM [6].

3.2. Joint Demosaicing Model

As mentioned above, to exploit the correlation between chromaticity and polarization in an RGB-Polarization image, the joint demosaicing problem can be formulated as to minimize the following energy function:

$$\min_{\mathbf{RC}, \mathbf{RP}} \|\mathbf{I} - \text{Mask}_{rgb} \mathbf{RC} - \text{Mask}_{pol} \mathbf{RP}\|_2^2 + \Phi(\mathbf{RP}) + \Psi(\mathbf{RC}), \quad (2)$$

where \mathbf{I} is the input RGB-Polarization mosaic image. Mask_{rgb} and Mask_{pol} represent the down-sample matrices of the chromatic and polarimetric information, respectively. The first term aims to maintain the accuracy between the input and reconstructed image. The latter two items designate the implicit priors imposed on \mathbf{RP}, \mathbf{RC} to regularize inference.

In this paper, we adopt the ADMM optimization scheme to recover the missing pixels in RGB and polarization channels. As the well-known idea of ADMM, we need to introduce the auxiliary variables \mathbf{P}, \mathbf{C} to Eq. 2 to constrain the problem. Then the problem can be formulated as the following optimization problem with both chromatic and polarization constraints:

$$\min_{\mathbf{RC}, \mathbf{RP}, \mathbf{C}, \mathbf{P}} \|\mathbf{I} - \text{Mask}_{pol} \mathbf{RP} - \text{Mask}_{rgb} \mathbf{RC}\|_2^2 + f(\mathbf{P}) + \mathbf{S}_{pol}^T (\mathbf{RP} - \mathbf{P}) + \frac{\rho_{pol}}{2} \|\mathbf{RP} - \mathbf{P}\|_2^2 + g(\mathbf{C}) + \mathbf{S}_{rgb}^T (\mathbf{RC} - \mathbf{C}) + \frac{\rho_{rgb}}{2} \|\mathbf{RC} - \mathbf{C}\|_2^2, \quad (3)$$

where $\mathbf{S}_{pol}, \mathbf{S}_{rgb}$ and ρ_{pol}, ρ_{rgb} are multipliers and penalty parameters for \mathbf{RC}, \mathbf{RP} . $f(\mathbf{P})$ and $g(\mathbf{C})$ are the implicit functions imposed on the desire results of \mathbf{P} and \mathbf{C} . Based on ADMM, we can get two sub-problems from Eq. 3 by splitting the variables \mathbf{P}, \mathbf{C} and \mathbf{RP}, \mathbf{RC} . The sub-problem about \mathbf{RP}, \mathbf{RC} can be formulated as:

$$\mathbf{RP}^{k+1}, \mathbf{RC}^{k+1} = \arg \min_{\mathbf{C}, \mathbf{P}} \|\mathbf{I} - \text{Mask}_{pol} \mathbf{RP} - \text{Mask}_{rgb} \mathbf{RC}\|_2^2 + \frac{\rho_{pol}}{2} \|\mathbf{RP} - (\mathbf{P}^k - y_{pol}^k)\|_2^2 + \frac{\rho_{rgb}}{2} \|\mathbf{RC} - (\mathbf{C}^k - y_{rgb}^k)\|_2^2, \quad (4)$$

The other sub-problem about \mathbf{P}, \mathbf{C} can be written as:

$$\begin{cases} \mathbf{P}^{k+1} = \arg \min_{\mathbf{P}} f(\mathbf{P}) + \frac{\rho_{pol}}{2} \|\mathbf{P} - (\mathbf{RP}^k + y_{pol}^k)\|_2^2, \\ \mathbf{C}^{k+1} = \arg \min_{\mathbf{C}} g(\mathbf{C}) + \frac{\rho_{rgb}}{2} \|\mathbf{C} - (\mathbf{RC}^k + y_{rgb}^k)\|_2^2, \end{cases} \quad (5)$$

where $y_{pol}^k = (1/\rho_{pol})\mathbf{S}_{pol}^{(k)}$, $y_{rgb}^k = (1/\rho_{rgb})\mathbf{S}_{rgb}^{(k)}$ are the scaled Lagrange multipliers.

4. Optimization

It found that the optimization can be iterated only if we obtained the desire value of variables \mathbf{P} , \mathbf{C} . Therefore, we define the $f(\mathbf{P}), g(\mathbf{C})$ with sparse coding and dictionary learning to obtain the approximate results for \mathbf{RP} , \mathbf{RC} , respectively.

4.1. Construct the Dictionaries

As we mentioned above, $f(\mathbf{P}), g(\mathbf{C})$ aim to obtain the desire reconstruction results of polarimetric and chromatic information. The performance of $f(\mathbf{P}), g(\mathbf{C})$ plays a key role during the iteration of optimization. Inspired by [1, 16, 17], sparse coding and dictionary learning can help to address this issue. In sparse and low-rank representations, constructing a proper dictionary is important. We use same strategy to construct the polarization dictionary \mathbf{D}_{pol} and the chromaticity dictionary \mathbf{D}_{rgb} . The difference between them is how to generate the corresponding signal data extracted from the RGB-Polarization dataset.

Generating the signal data. Before learning the dictionaries, we need to generate the corresponding signal data. The pipeline of signal data generation is illustrated in Fig. 2. We split the RGB-Polarization dataset into each channel and reorganize the polarimetric pixels recorded in R, G, B channels based on the RGB-Polarization pattern. Then we concatenate four reorganized polarization channels into polarimetric signal data with a size of $m \times n \times 4$. To learn the polarization dictionary and sparse code, we divide the polarimetric signal data into small patches with a size of 4×4 and randomly choose 114,000 of them. Then we lexicographically arrange the chosen patches as column vectors to generate the polarization signal data with a size of 64×114000 , denoted by \mathbf{Y}_{pol} .

We also need to generate the chromatic signal data for the chromatic dictionary. We can directly concatenate four full-resolution RGB-Polarization images from the RGB-Polarization dataset into a new form of data with a size of $m \times n \times 12$. Then we divide this new-form data into patches and rearrange them to column vectors as the signal data. The size of generated signal data is 192×114000 , denoted by \mathbf{Y}_{rgb} .

Learning the dictionaries. In this condition, we need to construct two over complete dictionaries for chromatic and polarimetric dictionaries as initialization. The dictionary can be obtained by solving the following optimization problem:

$$L(\mathbf{D}_\theta, \mathbf{X}) = \arg \min_{\mathbf{D}_\theta, \mathbf{X}} \|\mathbf{Y}_\theta - \mathbf{D}_\theta \mathbf{X}\|_2^2 + \lambda \|\mathbf{X}\|_1, \quad (6)$$

The number of atoms in \mathbf{D} is set to 256. The size of D_{pol}

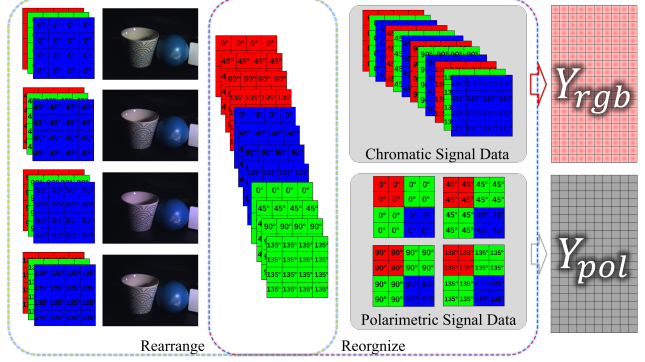


Figure 2. The generation of signal data for chromatic dictionary and polarimetric dictionary.

and D_{rgb} is 64×256 and 194×256 . \mathbf{X} is initial representation vector with size of $256 \times 114,000$. λ is L1 norm regularization parameter and set to 0.001 as shown in Tab. 3. According to K-SVD algorithm [1, 16], the optimization is solved by updating one of the parameters with the other variables fixed. After the iteration, we will obtain the learned dictionaries $\{\mathbf{D}_\theta | \theta \in (pol, rgb)\}$.

4.2. Update \mathbf{P} and \mathbf{C}

After obtaining the polarimetric and chromatic dictionaries, we can calculate the corresponding sparse coding to estimate the desire results of \mathbf{P} and \mathbf{C} .

Initialization: In the first iteration, we need to initialize the \mathbf{RP} and \mathbf{RC} . The size of the input mosaic image is $m \times n \times 1$. We reorganize pixels to one of the 12 channels based on the RGB-Polarization pattern which the size will be $m \times n \times 12$, as shown in Fig. 1. Then we use the Bicubic interpolation method to estimate the missing pixels, which is the preprocessing operation commonly used in the field of image super-resolution [12, 13, 39, 50]. Correspondingly, we use the same strategy to generate the signal data $\mathbf{Y} \in \{P, Q\}$. It should note that the initialization only applied in the first iteration. After the first iteration, the signal data $\mathbf{Y} \in \{P, Q\}$ should directly extract from \mathbf{RP} , \mathbf{RC} .

Calculating the sparse coding. As we mentioned before, the form of signal data $\mathbf{Y} \in \{P, Q\}$ can be sparsely represented. The polarimetric and chromatic sparse coding $\{\mathbf{X}_\theta | \theta \in (pol, rgb)\}$ are both sparse and low-rank. Furthermore, since the value of noise is sparse and non-negative, we also impose the non-negativity constraint on noise \mathbf{E}_θ . The calculation of polarization sparse coding \mathbf{X}_θ can be expressed as an optimization function:

$$\arg \min_{\mathbf{X}_\theta, \mathbf{E}_\theta} \text{rank}(\mathbf{X}_\theta) + \lambda \|\mathbf{E}_\theta\|_0 \quad (7)$$

$$s.t. \mathbf{Y} = \mathbf{D}_\theta \mathbf{X}_\theta + \mathbf{E}_\theta,$$

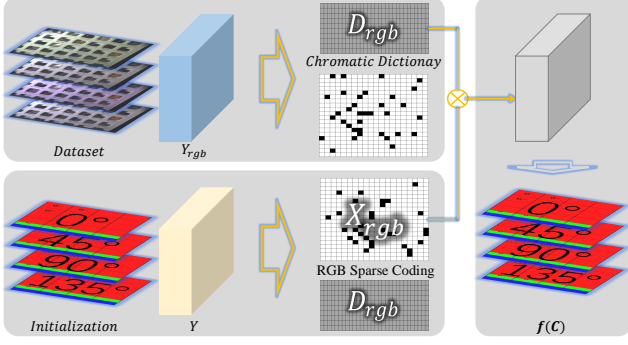


Figure 3. The pipeline of updating $f(C)$.

where λ is the parameter used to balance the effect of the noise components. We introduce J into Eq. 7:

$$\begin{aligned} \arg \min_{\mathbf{X}_\theta, \mathbf{E}_\theta, J} \|\mathbf{J}\|_* + \lambda \|\mathbf{E}_\theta\|_0 \\ \text{s.t. } \mathbf{Y} = \mathbf{D}_\theta \mathbf{X}_\theta + \mathbf{E}_\theta, \mathbf{X}_\theta = J, \end{aligned} \quad (8)$$

In this form, we can solve Eq. 8 by the well-known inexact ALM [36]. During the iteration, we use the OMP [45, 43] to select the best matching atom from the corresponding dictionary to construct sparse approximation.

Finally, the estimated \mathbf{P} and \mathbf{C} can be calculated by the dictionary (learned from the RGB-Polarization dataset) times the sparse coding (recovered from the output of initialization):

$$\begin{cases} f(\mathbf{P}) = \mathbf{D}_{pol} \times \mathbf{X}_{pol}, \\ f(\mathbf{C}) = \mathbf{D}_{rgb} \times \mathbf{X}_{rgb}, \end{cases} \quad (9)$$

After obtaining the value $f(\mathbf{P})$, $f(\mathbf{C})$, we can update the \mathbf{P} and \mathbf{C} according to Eq. 5. For the purpose of better illustration, the strategy of updating $f(\mathbf{C})$ is shown in Fig. 3 as an example.

4.3. Update \mathbf{RP} and \mathbf{RC}

We fix \mathbf{P} and \mathbf{C} and then use the ADMM algorithm to minimize the formula Eq. 4 rather than closed-form solution because it found that using optimization would yield better results. Then we can update \mathbf{RP} and \mathbf{RC} .

4.4. Update \mathbf{S}_{pol} and \mathbf{S}_{rgb}

Multipliers also need updating during each of the iteration. We firstly set the penalty parameters ρ_{rgb} and ρ_{pol} to 1.05. The update of scaled multipliers \mathbf{S}_{pol} and \mathbf{S}_{rgb} are as follows:

$$\begin{cases} \mathbf{S}_{pol}^{k+1} = \mathbf{S}_{pol}^k + \mathbf{RP}^{k+1} - \mathbf{P}^{k+1}, \\ \mathbf{S}_{rgb}^{k+1} = \mathbf{S}_{rgb}^k + \mathbf{RC}^{k+1} - \mathbf{C}^{k+1}, \end{cases} \quad (10)$$

Overall, the proposed optimization of joint chromatic and polarimetric demosaicing is summarized in Algorithm. 1.

Algorithm 1 Joint Chromatic and Polarimetric Demosaicing via Sparse Coding.

Input: Input RGB-Polarization mosaic image \mathbf{I} , ρ_{rgb} , ρ_{pol} ,
maxiter = 50, $\epsilon = 10^{-6}$

- 1: Construct the Dictionaries $\{\mathbf{D}_\theta | \theta \in (pol, rgb)\}$
- 2: initialization 4.2;
- 3: **for** $k = 1 : \text{maxiter}$ **do**
- 4: Updating \mathbf{P} and \mathbf{C} ;
- 5: Updating \mathbf{RP} and \mathbf{RC} ;
- 6: Updating \mathbf{S}_{pol} and \mathbf{S}_{rgb} ;
- 7: Break: $\{\|\mathbf{S}_{pol}^{k+1} - \mathbf{S}_{pol}^k\| < \epsilon \& \|\mathbf{S}_{rgb}^{k+1} - \mathbf{S}_{rgb}^k\| < \epsilon\}$
- 8: **end**

Output: \mathbf{RP} , \mathbf{RC}^*

After optimization, we will get the RGB-Polarization reconstruction \mathbf{RC} and arrange it into four full-resolution reconstructed RGB-Polarization images. As shown in Algorithm. 1, we will obtain two results \mathbf{RP} and \mathbf{RC} . However, the purpose of \mathbf{RP} is to constrain the reconstruction of polarimetric information during the optimization. It notes that the proposed method is based on the cross-optimization of RGB and polarization information. More experimental results demonstrate the effectiveness and performance of the proposed method.

5. Experiments

5.1. Experiment Settings

RGB-Polarization Dataset. The proposed method requires the ground-truth RGB-Polarization images to learn the dictionary. However, there is no such equipment ready to obtain the ground-truth RGB-Polarization images of real objects. Therefore, as shown in Fig. 4, we construct a data acquisition system by using a three-CMOS prism-based RGB camera, which is equipped with a mechanically motorized linear polarizer. The camera has a fixed white balancing setup, and the camera radiometric response is linear. We rotate the polarizer by 0, 45, 90 and 135 degrees under ordinary indoor light to acquire the dataset. The flickering effect of the fluorescent lamp will impact image acquisition, but the extent of this impact is limited. In addition, we lengthen the exposure time to reduce this influence.

The dataset we collected includes 105 scenes and 420 full three-channel 8-bit RGB images of 1456×1088 pixels. Based on the RGB-Polarization pattern shown in Fig. 1, the mosaic images are synthesized from the corresponding ground-truth images at four different polarization orientations and three RGB channels. We randomly choose 20 scenes as the testing set which will not be involved in the generation of the dictionary. One interesting observation from the data is that object color might change due to the polarization angle. This reveals the intrinsic corre-

lation of color and polarization for light reflected from an opaque surface. In turn, this phenomenon necessitates the joint chromatic and polarimetric demosaicing algorithm to account for this correlation.

Evaluation Metrics. The SSIM and PSNR are commonly used as the metrics for image evaluation. However, due to the introduction of polarization information, the Peak Signal to Noise Ratio(PSNR) and structural similarity index(SSIM [48]) are not enough for the evaluation metrics. In this case, we introduce the Stokes vector(S0), the degree of linear polarization(DoLP [20]) and angle of polarization(AoP [20]) to measure the accuracy of reconstructed polarization information. All these metrics are calculated by averaging four reconstructed images.

In addition, to verify the accurate reconstruction of chromaticity, we calculate the Euclidean distance between the reconstruction results and its ground-truth images in CIELab color space [10] to measure the color fidelity. Color Accuracy can be calculated as

$$\begin{aligned}
 \mathbf{CD} &= \frac{1}{mn} \sum_{i=1}^m \sum_{j=1}^n \|\mathbf{CY}(i, j) - \mathbf{CX}(i, j)\|_2 \\
 \mathbf{CA} &= -10 \cdot \lg\left(\frac{\mathbf{CD}}{255}\right),
 \end{aligned}
 \tag{11}$$

where m, n are the length and width of the image. **CD** and **CA** stand for Color Distance and Color Accuracy separately. **CY** and **CX** are the values calculated in CIELab color space by pixels of ground-truth images and reconstruction results.

5.2. Comparative Experiments

Since this is the first attempt on joint chromatic and polarimetric demosaicing which is based on a new type of array pattern, there are no prior results to compare with. In order to prove the effectiveness of our approach, the proposed methods are compared with the baseline interpolation algorithms such as Bicubic and Bilinear that have been proven effective in the image demosaicing processing field.

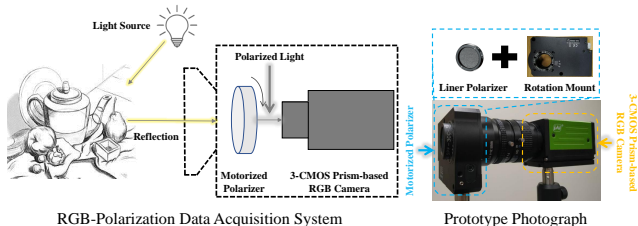


Figure 4. The hardware implementation of our designed data acquisition system. The system consists of a light source, a three-CMOS prism-based RGB camera, and a motorized polarizer with a rotation mount and a linear polarizer.

Method	PSNR	SSIM	CA	S0	DoLP	AoP
Bilinear	31.579	0.933	23.113	26.633	23.071	11.082
Bicubic	32.426	0.938	22.973	28.212	21.537	11.147
VDSR	32.661	0.926	22.217	19.907	19.449	10.088
RDN	34.219	0.955	23.925	28.160	15.078	8.665
Ours	35.078	0.943	23.473	31.833	23.657	11.152

Table 1. The results of comparisons. The best and the second results are in red and blue fonts.

In addition, we want to make comparisons with the state-of-art methods. However, unlike super-resolution, RGB demosaicing, and polarization demosaicing, our work focuses on a new filter array. It takes one channel RGB-Polarization mosaic image as input and recovers the other 11 channels ((r,g,b)*(0°, 45°, 90°, 135°)) for each pixel. Traditional algorithms for CFA or PFA cannot handle this very task. To make fair comparisons with VDSR [31] and RDN [54], we only modify the input and output as four RGB polarization images and keep their architecture unchanged. As shown in Tab. 1, the proposed method outperforms most methods in PSNR, SSIM, and Color Accuracy. However, the difference between the reconstruction results of RDN and ours seems to be minimal. RDN performs even better on SSIM and Color Accuracy than ours.

The well-known evaluation metrics (PSNR, SSIM, and color accuracy) are used to measure the accuracy of RGB information between the reconstructed image and the corresponding ground truth. The RDN builds a novel residual dense network to exploit the hierarchical feature from all the convolutional layers. Yet the polarimetric and chromatic information will be mixed and hard to exploit the feature separately. So based on the RGB information, RDN performs as good as the proposed method. However, we also need to concern the polarimetric information for the polarized color sensors. In this regard, we introduce S0, DoLP, and AoP to measure the accuracy of reconstructed polarization information. Based on the reconstructed four RGB images with polarization orientations, we can calculate the PSNR of S0, DoLP and AoP images(described in Sec. 5.1) of the scene. The results demonstrate that RDN cannot recover the polarization information as good as the proposed method, as shown in Tab. 2. The deep learning-based methods will estimate the polarimetric information by all data which includes chromatic information. As a result, RDN and VDSR perform even worse than the baseline interpolation methods on the evaluation metrics of polarization.

To compare with the sparse representation-based method proposed by Zhang [50], we consider each R, G, and B channel of the mosaic image as an input of their method and concatenate the outputs as a result in RGB form. However, the PCA with locally similar patches proposed by [50]

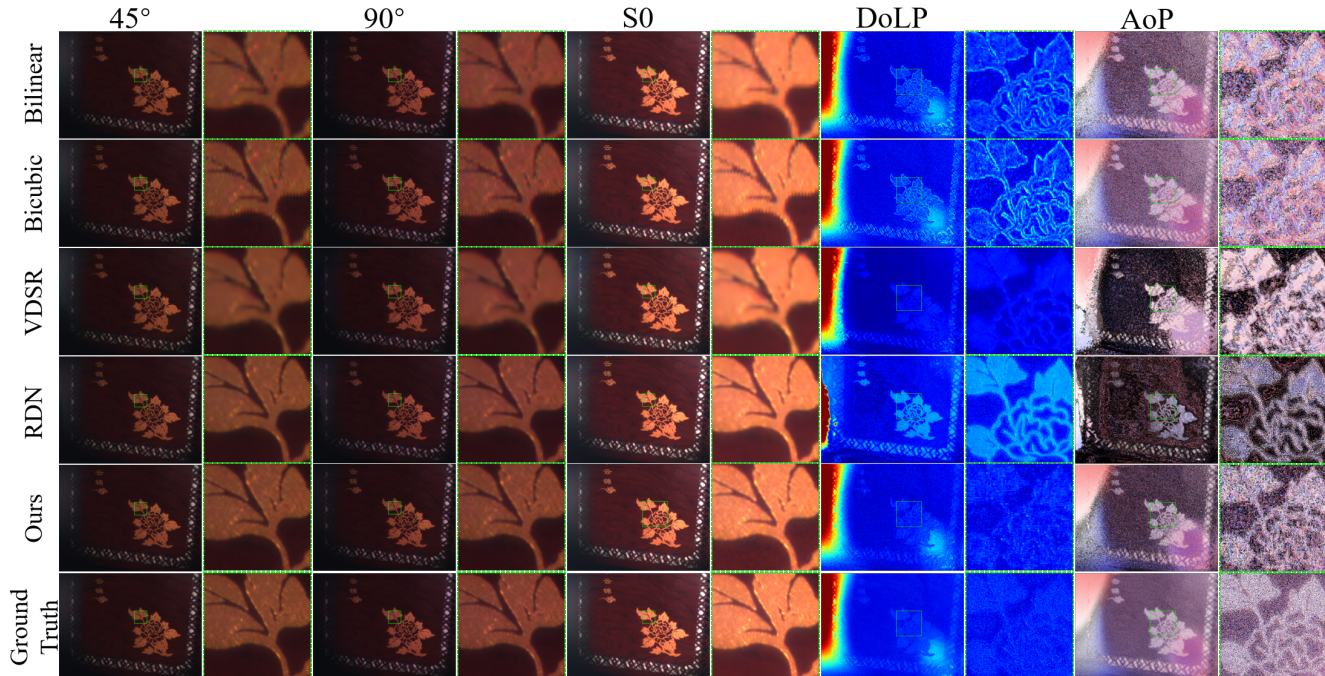


Figure 5. We randomly choose a scene for a sample of visual comparison. Reconstruction results of 45° , 90° , S0, DoLP, and AoP by Bilinear, Bicubic, RDN and our proposed method. Zooming in will show more details.

Method	PSNR	SSIM	CA	S0	DoLP	AoP	Time Consuming(s)
Zhang [50]	35.241	0.903	23.063	33.620	14.320	10.234	296.95
Ours	36.786	0.950	23.788	33.272	14.900	10.462	8.4385

Table 2. The results of comparisons with Zhang [50]’s method. It should be noted that the size of test images is 200×200

requires a lot of calculations. Therefore, there is literally a limit on the size of the target image. In our case, the resolution of the input image is 1456×1088 which can not be processed by the maximum array size. For a fair comparison, we cut the test images to 200×200 . As shown in Tab. 2, the method proposed by Zhang [50] can perform well in all evaluation metrics. However, the time consuming of Zhang [50] is very large and cannot be ignored.

The visualization of comparisons can be found in Fig. 5, from which we can perceive that the proposed method outperforms all other algorithms.

5.3. Controlled Experiments

Regularization Parameter. As shown in Tab. 3, the L1 norm regularization parameter will affect the performance of our proposed method. When the value of the L1 norm regularization parameter is 0.001, we can get better results.

Different Dictionary. Constructing appropriate dictionaries plays an important role in sparse representations and low-level vision task. A simple option would take the entire input data as the dictionary [37]. However, such a large

dictionary is computationally expensive and consumes too much storage space. In addition, the large dictionary ignores details of polarimetric and chromatic information in this ill-posed problem. As we mentioned before, we also train twelve dictionaries based on each channel of the RGB-Polarization data. Since there is no correlation between them during the demosaicing process, the reconstruction results are even worse. The results in Tab. 3 verify our theory.

Method	PSNR	SSIM	CA	S0	DoLP	AoP
1-Dic	32.057	0.906	21.881	29.799	17.824	8.505
12-Dic	30.758	0.879	21.103	27.862	10.756	4.468
$\lambda = 0.1$	31.579	0.933	23.113	29.810	19.783	10.730
$\lambda = 0.01$	32.426	0.938	22.973	31.219	20.570	10.252
$\lambda = 0.001$	35.078	0.943	23.473	31.833	22.777	11.152

Table 3. The results of controlled experiments

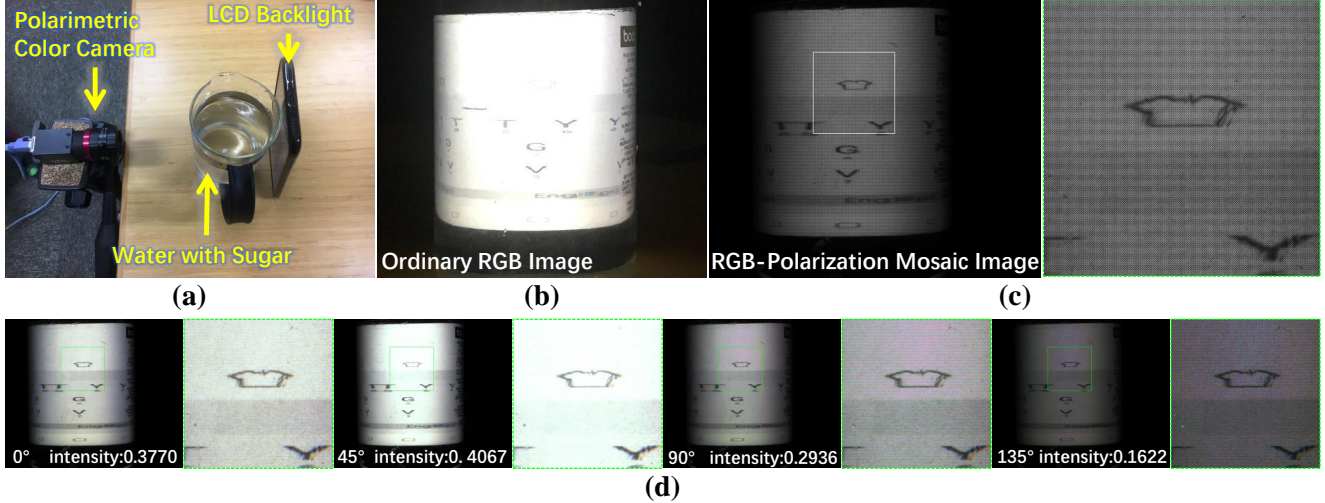


Figure 6. Application: (a) Application experiment setup; (b) An image of a glass of water with sugar recorded by a normal RGB camera; (c) An mosaic image of the same scene recorded by a polarimetric RGB camera(Lucid PHX050S-QC); (d) Four full-resolution RGB-Polarization images reconstruct by our method.

5.4. Real Image

Application. We conducted an application experiment to show the importance and effectiveness of joint color and polarization demosaicing. Industrially, the method of measuring the concentration of sugar in a solution is to observe how the sugar affects the polarization of the light. Although measuring the concentration of sugar requires not only the effect of the solution under polarized light but also many rigorous calibrations. Yet, observing the polarization declination is indeed one of the key steps in our joint demosaicing approach.

The traditional operation of rotating the polarizer not only causes deviation but also makes the experiment process cumbersome. As shown in Fig. 6, the ordinary RGB image taken with a normal camera can not display the color of polarized light that passes through a sugar solution. On the contrary, instead of shifting the polarization angle, the polarized color camera can directly capture the RGB-Polarization mosaic image by one snapshot. After processing along with the RGB-Polarization mosaic image by the proposed method, we can obtain **four polarization images with RGB information**. The ratio of the different value (calculated by RGB images) of known polarization angles (0° , 45° , 90° , and 135°) can help to calculate the concentration of sugar.

Real Scene. Polarimetric imagery can show the particular direction of the oscillation of the electric field described by the light. However, the ordinary RGB image taken with a normal camera can not display the color of polarized light. After the process of joint chromatic and polarimetric demosaicing, we can directly observe the color of the light in

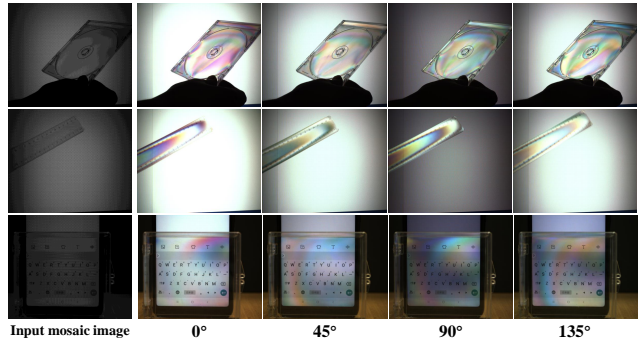


Figure 7. Experiment results in the real scene.

different angles of polarization orientation.

In this condition, we have captured images of a plastic box and a ruler in front of an LCD monitor. In addition, we also capture an image of the scene that the light of the screen passes through a plastic box. As shown in Fig. 7, the reconstruction results show the color of the differently polarized light with good quality. This further verifies that our proposed methods can handle joint demosaicing of real scenes.

6. Conclusion

In this paper, we first introduce joint chromatic and polarimetric demosaicing into the computer vision community. We build an RGB-Polarization data acquisition system by using a prism-based three-CMOS RGB camera and a motorized linear polarizer. As a very initial attempt, we propose a sparse representation-based demosaicing method by

jointly considering chromatic and polarimetric information. The experimental results demonstrate our proposed solution is effective and practical. As we have shown in the experiments on the real image, joint chromatic and polarimetric imaging can be a benefit to computer vision tasks. In the future, we will continue yielding improvements in imaging quality and optimizing runtime. Other future work aspects include demosaicing optimization and specific applications such as 3D modeling, intrinsic image decomposition, specular removal, object detection and recognition, and so on.

References

- [1] Michal Aharon, Michael Elad, Alfred Bruckstein, et al. K-svd: An algorithm for designing overcomplete dictionaries for sparse representation. *IEEE Transactions on signal processing*, 54(11):4311, 2006. 4
- [2] Ashfaq Ahmed, Xiaojin Zhao, Viktor Gruev, Junchao Zhang, and Amine Bermak. Residual interpolation for division of focal plane polarization image sensors. *Optics express*, 25(9):10651–10662, 2017. 2
- [3] Sanaz Alali and I Alex Vitkin. Polarized light imaging in biomedicine: emerging mueller matrix methodologies for bulk tissue assessment. *Journal of biomedical optics*, 20(6):061104, 2015. 2
- [4] David Alleysson, Sabine Susstrunk, and Jeanny Hérault. Linear demosaicing inspired by the human visual system. *IEEE Transactions on Image Processing*, 14(4):439–449, 2005. 2
- [5] Bryce E Bayer. Color imaging array. July 20 1976. US Patent 3,971,065. 1
- [6] Stephen Boyd, Neal Parikh, Eric Chu, Borja Peleato, Jonathan Eckstein, et al. Distributed optimization and statistical learning via the alternating direction method of multipliers. *Foundations and Trends® in Machine learning*, 3(1):1–122, 2011. 3
- [7] Antoni Buades, Bartomeu Coll, Jean-Michel Morel, and Catalina Sbert. Self-similarity driven color demosaicking. *IEEE Transactions on Image Processing*, 18(6):1192–1202, 2009. 2
- [8] Chen Chen, Qifeng Chen, Jia Xu, and Vladlen Koltun. Learning to see in the dark. pages 3291–3300, 2018. 2
- [9] Laurent Condat and Saleh Mosaddegh. Joint demosaicking and denoising by total variation minimization. pages 2781–2784, 2012. 2
- [10] Christine Connolly and T Fleiss. A study of efficiency and accuracy in the transformation from rgb to ciela color space. *IEEE Transactions on Image Processing*, 6(7):1046–1048, 1997. 6
- [11] Akshat Dave, Anil Kumar, Kaushik Mitra, et al. Compressive image recovery using recurrent generative model. pages 1702–1706, 2017. 2
- [12] Weisheng Dong, Lei Zhang, Guangming Shi, and Xin Li. Nonlocally centralized sparse representation for image restoration. *IEEE Transactions on Image Processing*, 22(4):1620–1630, 2013. 4
- [13] Weisheng Dong, Lei Zhang, Guangming Shi, and Xiaolin Wu. Image deblurring and super-resolution by adaptive sparse domain selection and adaptive regularization. *IEEE Transactions on Image Processing*, 20(7):1838–1857, 2011. 4
- [14] Florence Drouet, Christophe Stolz, Olivier Laligant, and Olivier Aubreton. 3d reconstruction of external and internal surfaces of transparent objects from polarization state of highlights. *Optics letters*, 39(10):2955–2958, 2014. 2
- [15] Eric Dubois. Frequency-domain methods for demosaicking of bayer-sampled color images. *IEEE Signal Processing Letters*, 12(12):847–850, 2005. 2
- [16] Bogdan Dumitrescu and Paul Irofti. Regularized k-svd. *IEEE Signal Processing Letters*, 24(3):309–313, 2017. 4
- [17] Michael Elad and Michal Aharon. Image denoising via sparse and redundant representations over learned dictionaries. *IEEE Transactions on Image processing*, 15(12):3736–3745, 2006. 4
- [18] Shuai Fang, XiuShan Xia, Xing Huo, and ChangWen Chen. Image dehazing using polarization effects of objects and airlight. *Optics express*, 22(16):19523–19537, 2014. 2
- [19] Shengkui Gao and Viktor Gruev. Bilinear and bicubic interpolation methods for division of focal plane polarimeters. *Optics express*, 19(27):26161–26173, 2011. 1
- [20] Shengkui Gao and Viktor Gruev. Gradient-based interpolation method for division-of-focal-plane polarimeters. *Optics express*, 21(1):1137–1151, 2013. 1, 6
- [21] Pascal Getreuer. Zhang-wu directional lmmse image demosaicking. *Image Processing On Line*, 1:117–126, 2011. 1
- [22] Michaël Gharbi, Gaurav Chaurasia, Sylvain Paris, and Frédéric Durand. Deep joint demosaicking and denoising. *ACM Transactions on Graphics (TOG)*, 35(6):191, 2016. 2
- [23] Jinwook Go, Kwanghoon Sohn, and Chulhee Lee. Interpolation using neural networks for digital still cameras. *IEEE Transactions on Consumer Electronics*, 46(3):610–616, 2000. 2
- [24] Felix Heide, Steven Diamond, Matthias Nießner, Jonathan Ragan-Kelley, Wolfgang Heidrich, and Gordon Wetzstein. Proximal: Efficient image optimization using proximal algorithms. *ACM Transactions on Graphics (TOG)*, 35(4):84, 2016. 2
- [25] Theodor Heinze, Martin von Löwis, and Andreas Polze. Joint multi-frame demosaicing and super-resolution with artificial neural networks. pages 540–543, 2012. 1, 2
- [26] Bernardo Henz, Eduardo SL Gastal, and Manuel M Oliveira. Deep joint design of color filter arrays and demosaicing. 37(2):389–399, 2018. 2
- [27] Fei Hu, Yayun Cheng, Liangqi Gui, Liang Wu, Xinyi Zhang, Xiaohui Peng, and Jinlong Su. Polarization-based material classification technique using passive millimeter-wave polarimetric imagery. *Applied optics*, 55(31):8690–8697, 2016. 2
- [28] Sunil Prasad Jaiswal, Oscar C Au, Vinit Jakhethiya, Yuan Yuan, and Haiyan Yang. Exploitation of inter-color correlation for color image demosaicking. pages 1812–1816, 2014. 2
- [29] Oren Kapah and Hagit Zabrodsky Hel-Or. Demosaicking using artificial neural networks. 3962:112–121, 2000. 2

- [30] S Kaur and Vijay Kumar Banga. A survey of demosaicing: Issues and challenges. *International Journal of Science, Engineering and Technologies*, 2(1):2, 2015. 2
- [31] Jiwon Kim, Jung Kwon Lee, and Kyoung Mu Lee. Accurate image super-resolution using very deep convolutional networks. In *Proceedings of the IEEE conference on computer vision and pattern recognition*, pages 1646–1654, 2016. 6
- [32] Teresa Klatzer, Kerstin Hammernik, Patrick Knobelreiter, and Thomas Pock. Learning joint demosaicing and denoising based on sequential energy minimization. pages 1–11, 2016. 2
- [33] Xin Li. Demosaicing by successive approximation. *IEEE Transactions on Image Processing*, 14(3):370–379, 2005. 2
- [34] Xin Li, Bahadır Gunturk, and Lei Zhang. Image demosaicing: A systematic survey. 6822:68221J, 2008. 2
- [35] Nai-Xiang Lian, Lanlan Chang, Yap-Peng Tan, and Vitali Zagorodnov. Adaptive filtering for color filter array demosaicking. *IEEE Transactions on Image Processing*, 16(10):2515–2525, 2007. 2
- [36] Zhouchen Lin, Minming Chen, and Yi Ma. The augmented lagrange multiplier method for exact recovery of corrupted low-rank matrices. *arXiv preprint arXiv:1009.5055*, 2010. 5
- [37] Guangcan Liu, Zhouchen Lin, and Yong Yu. Robust subspace segmentation by low-rank representation. In *ICML*, volume 1, page 8, 2010. 7
- [38] Yangjing Long and Yizhen Huang. Adaptive demosaicking using multiple neural networks. pages 353–357, 2006. 2
- [39] Julien Mairal, Francis Bach, Jean Ponce, Guillermo Sapiro, and Andrew Zisserman. Non-local sparse models for image restoration. pages 2272–2279, 2009. 1, 2, 3, 4
- [40] Daniele Menon and Giancarlo Calvagno. Color image demosaicking: An overview. *Signal Processing: Image Communication*, 26(8-9):518–533, 2011. 2
- [41] Sofiane Mihoubi, Pierre-Jean Lapray, and Laurent Bigué. Survey of demosaicking methods for polarization filter array images. *Sensors*, 18(11):3688, 2018. 2
- [42] Abdolreza Abdolhosseini Moghadam, Mohammad Aghagolzadeh, Mrityunjay Kumar, and Hayder Radha. Compressive framework for demosaicing of natural images. *IEEE transactions on image processing*, 22(6):2356–2371, 2013. 2
- [43] Yagyensh Chandra Pati, Ramin Rezaiifar, and Perinkulam Sambamurthy Krishnaprasad. Orthogonal matching pursuit: Recursive function approximation with applications to wavelet decomposition. pages 40–44, 1993. 5
- [44] Bradley M Ratliff, Charles F LaCasse, and J Scott Tyo. Interpolation strategies for reducing ifov artifacts in microgrid polarimeter imagery. *Optics express*, 17(11):9112–9125, 2009. 1, 2
- [45] Joel A Tropp and Anna C Gilbert. Signal recovery from random measurements via orthogonal matching pursuit. *IEEE Transactions on information theory*, 53(12):4655–4666, 2007. 5
- [46] J Scott Tyo, Charles F LaCasse, and Bradley M Ratliff. Total elimination of sampling errors in polarization imagery obtained with integrated microgrid polarimeters. *Optics letters*, 34(20):3187–3189, 2009. 2
- [47] Yi-Qing Wang. A multilayer neural network for image demosaicking. pages 1852–1856, 2014. 1, 2
- [48] Zhou Wang, Alan C Bovik, Hamid R Sheikh, Eero P Simoncelli, et al. Image quality assessment: from error visibility to structural similarity. *IEEE transactions on image processing*, 13(4):600–612, 2004. 6
- [49] Junchao Zhang, Haibo Luo, Bin Hui, and Zheng Chang. Image interpolation for division of focal plane polarimeters with intensity correlation. *Optics express*, 24(18):20799–20807, 2016. 1, 2
- [50] Junchao Zhang, Haibo Luo, Rongguang Liang, Ashfaq Ahmed, Xiangyue Zhang, Bin Hui, and Zheng Chang. Sparse representation-based demosaicing method for microgrid polarimeter imagery. *Optics letters*, 43(14):3265–3268, 2018. 1, 2, 3, 4, 6, 7
- [51] Junchao Zhang, Jianbo Shao, Haibo Luo, Xiangyue Zhang, Bin Hui, Zheng Chang, and Rongguang Liang. Learning a convolutional demosaicing network for microgrid polarimeter imagery. *Optics letters*, 43(18):4534–4537, 2018. 1, 3
- [52] Lei Zhang and Xiaolin Wu. Color demosaicking via directional linear minimum mean square-error estimation. *IEEE Transactions on Image Processing*, 14(12):2167–2178, 2005. 2
- [53] Lei Zhang, Xiaolin Wu, Antoni Buades, and Xin Li. Color demosaicking by local directional interpolation and nonlocal adaptive thresholding. *Journal of Electronic imaging*, 20(2):023016, 2011. 2
- [54] Yulun Zhang, Yapeng Tian, Yu Kong, Bineng Zhong, and Yun Fu. Residual dense network for image super-resolution. In *Proceedings of the IEEE Conference on Computer Vision and Pattern Recognition*, pages 2472–2481, 2018. 6